ACS APPLIED MATERIALS & INTERFACES

Research Article

www.acsami.org

Selective Uptake of Rare Earths from Aqueous Solutions by EDTA-Functionalized Magnetic and Nonmagnetic Nanoparticles

David Dupont,[†] Ward Brullot,[‡] Maarten Bloemen,[‡] Thierry Verbiest,[‡] and Koen Binnemans*[,†]

[†]Molecular Design and Synthesis, Department of Chemistry, KU Leuven, Celestijnenlaan 200F, P.O. Box 2404, B-3001 Heverlee, Belgium

[‡]Molecular Imaging and Photonics, Department of Chemistry, KU Leuven, Celestijnenlaan 200D, P.O. Box 2425, B-3001 Heverlee, Belgium

Supporting Information

ABSTRACT: Magnetic (Fe_3O_4) and nonmagnetic (SiO_2 and TiO_2) nanoparticles were decorated on their surface with *N*-[(3-trimethoxysilyl)propyl]ethylenediamine triacetic acid (TMS-EDTA). The aim was to investigate the influence of the substrate on the behavior of these immobilized metal coordinating groups. The nanoparticles functionalized with TMS-EDTA were used for the adsorption and separation of trivalent rare-earth ions from aqueous solutions. The general adsorption capacity of the nanoparticles was very high (100 to 400 mg/g) due to their large surface area. The heavy rare-earth ions are known to have a higher affinity for the coordinating groups than the light rare-earth ions but an additional difference in selectivity was observed between the different nanoparticles. The separation of pairs of rare-earth ions was found to be dependent on the substrate, namely the density of EDTA groups on the surface. The observation that sterical hindrance (or crowding) of immobilized ligands influences the selectivity could provide a new tool for the fine-tuning of the coordination ability of traditional chelating ligands.

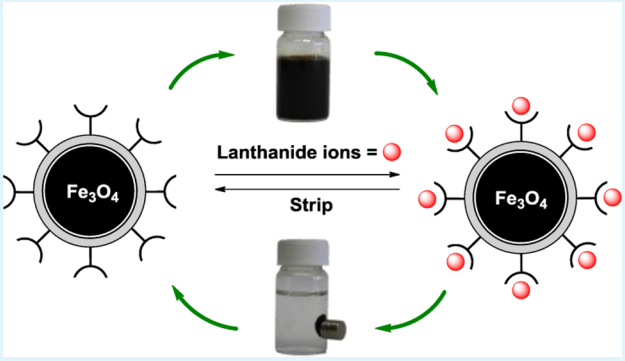

KEYWORDS: *EDTA, lanthanides, magnetic nanoparticles, magnetite, metal recovery, rare earths*

1. INTRODUCTION

Magnetic nanoparticles are very popular advanced materials.[1,2] The possibility to guide these particles magnetically to recover them from solution by a magnet and to functionalize their surface with a large variety of functional groups has led to their application in biomedicine, homogeneous catalysis, wastewater processing and many other technological fields.[3−14] Biomedical applications include targeted drug delivery, biosensors and dual imaging by lanthanide ions attached to magnetic nanoparticles.[3−5] Functionalized magnetic nanoparticles are also excellent candidates for the selective extraction of metal traces from wastewater streams or industrial effluents.[6−15] These sophisticated adsorbents can act toward metal ions as a kind of "nanosponges" and they can easily be retrieved from solution with a magnet (Figure 1). After the adsorbed ions are stripped, the nanoparticles can be reused, making this a promising sustainable and green technology. The recovery of heavy metals and precious metals with functionalized nanoparticles has been studied extensively,[6−14] but the recovery of rare earths by nanoparticles has received far less attention.[16] Core−shell nanoparticles with magnetic (Fe_3O_4) cores and SiO_2 or TiO_2 shells are also excellent candidates for this type of applications.[8,9,15,17] These SiO_2 or TiO_2 shells can be functionalized with metal coordinating groups and they would greatly benefit from a better insight into the influence of the substrate on the behavior of the metal coordinating groups on their surface. This paper reports on the differences in adsorption and separation of lanthanide ions by *N*-[(3-trimethoxysilyl)propyl]ethylenediamine triacetic acid (TMS-EDTA) attached to Fe_3O_4, SiO_2 or TiO_2 surfaces.

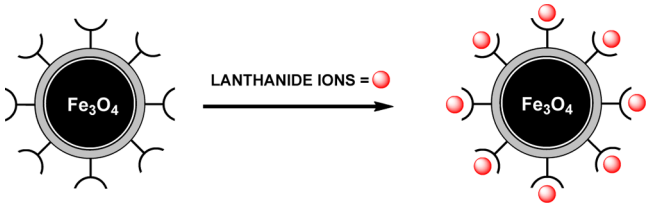

Figure 1. Schematic representation of the capture of lanthanide ions by functionalized magnetic nanoparticles.

Silane chemistry is a powerful tool to anchor functional groups on the surface of nanoparticles.[18−22] The large number of commercially available trialkoxysilanes with functional groups offers unique possibilities for the surface-modification of oxide nanoparticles.[15,18−22] The silane groups form strong

Received: December 29, 2013
Accepted: March 17, 2014
Published: March 18, 2014

covalent bonds with the hydroxyl groups on the surface of oxide nanoparticles and increase their stability in solution.[21] TMS-EDTA allows functionalization of oxide nanoparticles with EDTA functional groups for coordination of metal ions. The covalently bonded TMS-EDTA yields nanoparticles with a much better long-term stability and resistance to acidic conditions than nanoparticles where EDTA is directly bonded to the surface by weak electrostatic interactions.[7,10] Although the selectivity of traditional complexing agents such as EDTA and DTPA toward different metal ions is well understood in aqueous solutions, this is not the case for the behavior of their analogues attached to a surface. The density of immobilized coordination groups on a surface can be high and the steric hindrance (crowding) can alter the selectivity of the coordination groups, which creates new opportunities for the fine-tuning of the ligand selectivity. This possibility of fine-tuning of the ligand selectivity is of importance for the difficult separation of rare-earth ions. Most extractants (e.g., tributyl phosphate (TBP) and di-(2-ethylhexyl)phosphoric acid (DEHPA)) and chelating agents (e.g., EDTA and diethylene triamine pentaacetic acid (DTPA)) have an increased affinity for the heavier rare-earth ions, due to the smaller ionic radii and higher charge densities of the heavy rare-earth ions.[23,24] Unfortunately, the difference in ionic radius between neighboring rare-earth elements is small, making an efficient sized-based separation very challenging.[23] Progress has been made in the development of more selective extractants for liquid/liquid extraction of rare earths, but the separation is still inefficient.[23,25]

In this paper, a new approach is proposed to tune the selectivity of existing ligands and extractants. The selectivity is achieved by combining the inherent selectivity of EDTA groups with the steric hindrance of coordinating groups on the surface of oxide nanoparticles. Magnetic (Fe_3O_4) and nonmagnetic (TiO_2 and SiO_2) nanoparticles were functionalized with TMS-EDTA. These oxides were selected because they have different densities of OH groups on their surfaces. The OH density increases in the order Fe_3O_4 < TiO_2 < SiO_2.[26−29] Higher densities of OH groups should result in higher densities of EDTA groups on the nanoparticles, because the silanes react with these hydroxyl groups. The functionalized nanoparticles were characterized extensively and their behavior in solution was investigated both for the adsorption and the separation of rare-earth ions by selective uptake.

2. EXPERIMENTAL SECTION

Chemicals. Anhydrous $FeCl_3$ (97%), SiO_2 nanoparticles (12 nm, 99.5%), TiO_2 nanoparticles (21 nm, 99.5%), $Y(NO_3)_3{\cdot}6H_2O$ (99.9%) and $Lu(NO_3)_3{\cdot}5H_2O$ (99.9%) were purchased from Sigma-Aldrich. *N*-[(3-Trimethoxysilyl)propyl]ethylenediamine triacetic acid trisodium salt (TMS-EDTA) (45 wt %) was purchased from ABCR chemicals, HCl (32 wt %), methanol (HPLC grade) and NaOH (97%) were purchased from VWR. $Sm(NO_3)_3{\cdot}6H_2O$ (99.9%), $Gd(NO_3)_3{\cdot}6H_2O$ (99.9%), $Er(NO_3)_3{\cdot}5H_2O$ (99.9%) and *n*-octylamine (NOA) (99.9%) were purchased from Acros Chemicals. $La(NO_3)_3{\cdot}6H_2O$ (99.9%) and $Pr(NO_3)_3{\cdot}6H_2O$ (99.9%) were purchased from Chempur. $Nd(NO_3)_3{\cdot}6H_2O$ (99.9%), $Tb(NO_3)_3{\cdot}5H_2O$ (99.9%), $Dy(NO_3)_3{\cdot}5H_2O$ (99.9%), $Ho(NO_3)_3{\cdot}5H_2O$ (99.9%) and $Yb(NO_3)_3{\cdot}5H_2O$ (99.9%) were purchased from Alfa Aesar. All chemical were used as received without further purification.

Equipment and Characterization. A Branson 5510 (10 L) and a Branson 2510 MTH (3 L) sonicator bath were used to disperse nanoparticles in a solvent. A mechanical shaker (IKA KS 130 basic with universal attachment) was employed during adsorption experiments and a vibrating plate (IKA MS 3 basic) was used in the sample preparation for TXRF analysis. Finally, a centrifuge (Heraeus labofuge 200) was used to separate the nonmagnetic nanoparticles from solution. Transmission Electron Microscopy (TEM) was carried out on a JEOL JEM2100 apparatus using an acceleration voltage of 80 or 200 kV. The size determination was done using ImageJ software. Magnetization data were obtained from vibrating sample magnetometry (VSM) experiments performed on a VSM Maglab setup from Oxford Instruments at 300 K. Fourier Transform Infrared (FTIR) spectra were measured between 5000 and 400 cm^{-1} on a Bruker Vertex 70 spectrometer, with a Platinum ATR module. Thermogravimetric analysis (TGA) was performed with a TA Instruments Q600 thermogravimeter, measuring from 25 to 1300 °C (10 °C per minute, argon atmosphere). Finally, the carbon, hydrogen and nitrogen contents of the functionalized nanoparticles were determined by CHN elemental analysis with a CE Instruments EA-1110 elemental analyzer. The hydrodynamic properties and of the nanoparticles were probed by dynamic light scattering (DLS) and ζ-potential measurements using a Brookhaven 90Plus particle analyzer with the scattering angle set at 90°. The acidity of the EDTA groups was investigated with a Mettler-Toledo T90 automatic titrator using HCl (0.01 M) and NaOH (0.01 M) as the titrant. Total reflection X-ray fluorescence (TXRF) analysis was used to measure the rare-earth concentrations. A benchtop Bruker S2 PICOFOX TXRF spectrometer equipped with a molybdenum X-ray source was used. Rare-earth concentrations were measured directly on the nanoparticle dispersion, which is a major advantage of TXRF compared to inductively coupled plasma mass spectrometry analysis where nanoparticles have to be disintegrated in acid prior to analysis. For the sample preparation, Eppendorf microtubes were filled with an amount of sample solution and a similar concentration (10 to 100 mg/L) of Ga^{3+} as internal standard (1000 ppm gallium dissolved in 2−3% HNO_3, Merck). Gallium was chosen because this element has a high sensitivity and does not interfere with the lanthanide signals. Finally, a 5 μL drop of this solution was put on a quartz plate, previously treated with a silicone/isopropanol solution (Serva) and dried for 15 min at 60 °C prior to analysis. Each sample was measured for 200 s.

Synthesis of Precursor Magnetite Nanoparticles. A well-described in-house synthesis procedure was followed for the synthesis of the magnetite nanoparticles.[30] First, ethylene glycol (37.5 mL) and *n*-octylamine (NOA) (25 mL) were poured into a flask and heated to 150 °C. At the same time, $FeCl_3$ (2.4 g) was dissolved in a beaker containing ethylene glycol (10 mL) and Milli-Q water (3.5 mL). Once $FeCl_3$ was totally dissolved, the iron(III)-containing solution was slowly added to the flask with ethylene glycol and *n*-octylamine and further heated to reflux at 180 °C for 24 h. After reaction, the obtained particles were precipitated from the reaction mixture by a NdFeB magnet and washed three times with acetone. Finally, they were dried in vacuo at room temperature for 20 min to obtain a black powder of Fe_3O_4(NOA) nanoparticles with a typical yield of 1 g.

Silanization of Nanoparticles. Fe_3O_4(NOA), TiO_2 and SiO_2 nanoparticles were functionalized with TMS-EDTA. The Fe_3O_4(NOA) nanoparticles were used as such, but the TiO_2 and SiO_2 nanoparticles were dried at 50 °C in vacuo for 24 h. The silanization protocol started by dissolving 100 mg of nanoparticles in MeOH (100 mL). The beaker was placed in an ultrasonic bath for 2 h. TMS-EDTA (1 mmol) was then added together with a few drops of glacial acetic acid. The beaker was placed for another 2 h in the ultrasonic bath. The particles were precipitated from the reaction mixture by a small magnet or a centrifuge (5300 rpm, 15 min) and washed one time with water and two times with acetone. Finally, they were dried in vacuo at room temperature for 20 min, resulting in Fe_3O_4(TMS-EDTA), TiO_2(TMS-EDTA) and SiO_2(TMS-EDTA).

Procedure for Adsorption, Separation and Stripping Experiments. Functionalized nanoparticles (5 mg) were dissolved in Milli-Q water (10 mL) by placing the solution in an ultrasonic bath for 1 h. The vials were then taken out and the desired volume of equimolar, binary rare-earth solution (5×10^{-3} M) was added. These mixtures of rare earths pairs were prepared in advance by combining and diluting concentrated stock solutions of the individual rare-earth elements (0.05 M). All the concentrations were verified by total reflection X-ray fluorescence (TXRF). The pH was set using HCl (0.1 M) or NaOH

(0.1 M). The vials were then placed on a mechanical shaker for 24 h to ensure equilibrium was reached. The particles were settled using a small NdFeB magnet in the case of magnetic nanoparticles or a centrifuge (5300 rpm, 20 min) in the case of nonmagnetic nanoparticles. The solution was removed and the nanoparticles were washed two times with acetone in order not to influence the adsorption equilibrium. The rare-earth content on the nanoparticles was then analyzed with TXRF. The stripping of rare-earth ions from the nanoparticles was done by redispersing the washed nanoparticles in water and lowering the pH to 2.75 by an HCl solution (0.1 M). After 1 h, the nanoparticles were retrieved, washed and analyzed using TXRF.

3. RESULTS AND DISCUSSION

Magnetic Nanoparticles. The magnetite nanoparticles were synthesized using a forced hydrolysis method.[30] The nanoparticles were of high quality, in the sense that they had a high saturation magnetization (66 emu/g) and a relatively well-defined spherical shape (TEM) The *n*-octylamine layer on the precursor nanoparticles is weakly bonded and can be replaced by a covalently bonded layer of functional silanes. The silanes are first hydrolyzed to silanols, which react with the hydroxyl groups on the surface of the nanoparticles in a condensation reaction. The resulting product was a black powder with an excellent shelf life. Magnetite nanoparticles functionalized with EDTA-silane (Figure 2) will be referred to as Fe_3O_4(TMS-EDTA). Commercially available SiO_2 and TiO_2 nanoparticles were dried prior to use. Drying the particles before silanization and then redispersing them in water increases the surface coverage.[26] This procedure and the influence of the concentration surface hydroxyl groups on the silanization of SiO_2 were studied extensively by Dugas et al.[26] For magnetite (Fe_3O_4) nanoparticles, this step was not necessary because the precursor particles had a hydrophobic *n*-octylamine coating. The silanization was carried out in the same way as for the magnetite nanoparticles. The final products were white powders that will be referred to as SiO_2(TMS-EDTA) and TiO_2(TMS-EDTA).

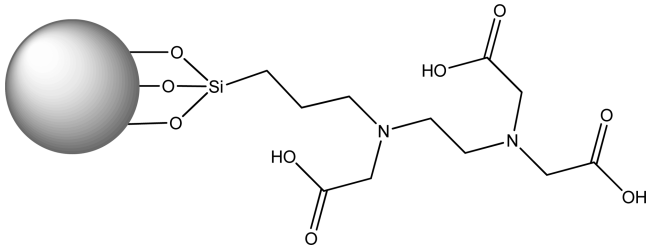

Figure 2. Nanoparticle functionalized with TMS-EDTA.

Characterization of the Nanoparticles. The TEM images (Figures S5–S7, Supporting Information) showed that the Fe_3O_4 particles had a relatively spherical shape and were monodisperse with an average core diameter of (10.5 ± 1.8) nm. The SiO_2 nanoparticles and TiO_2 were more polydisperse and had a diameter of (16.6 ± 5.8) nm and (17.9 ± 5.9) nm, respectively. Vibrating Sample Magnetometry (VSM) measurements (Figure S4, Supporting Information) showed that the magnetic nanoparticles had a saturation magnetization of 66 emu/g and negligible coercivity and remanent magnetization, indicating superparamagnetic behavior. This property allows for convenient retrieval of the nanoparticles from solution, using only a permanent magnet (Figure 3). Full retrieval (>99.9%) was possible in less than 10 s.

Figure 3. Fe_3O_4(TMS-EDTA) nanoparticles dispersed in water (left) and the retrieval using a permanent magnet (right).

The presence of EDTA on the nanoparticles was verified using FTIR spectroscopy (Figure S1–S3, Supporting Information). EDTA has two strong absorption bands between 1570–1610 cm^{-1} and 1350–1450 cm^{-1}.[19,21] These bands occur as a pair and can be assigned to asymmetrical and symmetrical COO^- stretching vibrations, respectively. Fe_3O_4(TMS-EDTA) has IR absorption bands at 1592 and 1401 cm^{-1}, TiO_2(TMS-EDTA) at 1594 and 1404 cm^{-1} and SiO_2(TMS-EDTA) at 1591 and 1408 cm^{-1}. Si–O–Si bands due to oligomerization of the silanes can be found between 1150 and 1000 cm^{-1} and the Si–O–M bonds (M = Fe, Si, Ti) bonds cause a strong band between 900 and 1000 cm^{-1}, depending on the metal.[19,21,31] For Fe_3O_4(TMS-EDTA), these bands were found at 1091 and 903 cm^{-1}, respectively, for TiO_2(TMS-EDTA) at 1090 and 919 cm^{-1} and for SiO_2(TMS-EDTA) only one band at 1062 cm^{-1} because M = S. The lattice vibration band of the core broadens and shifts, due to the formation of Si–O–M (M = Fe, Si, Ti) bonds in the silane surface layer and was found at 548 cm^{-1} for Fe_3O_4, 430 cm^{-1} for TiO_2 and 802 cm^{-1} for SiO_2. Other features include the weak asymmetric and symmetric CH2 stretchings at 2922–2931 and 2852–2856 cm^{-1}.[17,19]

The EDTA-silane groups and the free hydroxyl groups on the oxide surface of the nanoparticle core can form positively or negatively charged species, depending on the pH. Surface hydroxyl groups on Fe_3O_4, TiO_2 and SiO_2 show amphoteric behavior and have a point of zero charge around pH 7, pH 6.5 and pH 2.2, respectively.[32–34] These charges are negligible though, compared to the many charges of the TMS-EDTA groups. TMS-EDTA contains five sites with acid–base behavior: two tertiary amines and three carboxylic acid groups (Figure 4). The positively charged species are often omitted because these only occur at very low pH.

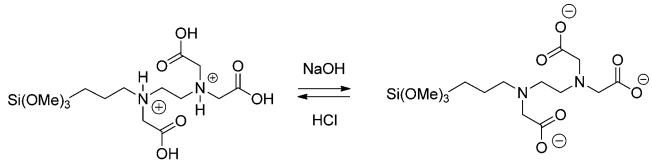

Figure 4. Structure of TMS-EDTA in its most positively and negatively charged state.

Knowing the pK_a values of TMS-EDTA is important because these determine the speciation of TMS-EDTA as function of pH. Because no pK_a values were found for TMS-EDTA in the literature, a titration was carried out to determine the pK_a values of TMS-EDTA on the nanoparticles. The pK_a of the pure silane cannot be determined because the silane would hydrolyze in water and react with the glass of the pH electrode.

The pK_a values for EDTA-silane (TMS-EDTA) attached to a Fe_3O_4 nanoparticle were found to be pK_{a1} = 4.17, pK_{a2} = 6.89, pK_{a3} = 10.00. The pK_a values of the positively charged species could not be determined because of the instability at pH ≤ 2.5; ζ-potential measurements (Figure S9, Supporting Information) for a dispersion of Fe_3O_4(TMS-EDTA) nanoparticles showed that the negative charge on the particles increases with pH because the carboxylic acid groups are gradually deprotonated. The point of zero charge (PZC) is situated at pH 2.8, where all the carboxylic acid groups are fully protonated. If the ionic strength of the solution is raised too much, the absolute value of the ζ-potential diminishes, causing aggregation and/or sedimentation. The application of functionalized nanoparticles as sorbents is therefore limited to the adsorption of low or trace metal concentrations.[6−14] Dynamic light scattering (DLS) was carried out to measure the hydrodynamic radii and the polydispersity (aggregation) of the nanoparticles at different pH values (Table S1, Supporting Information). The increase in hydrodynamic radius with pH confirmed that the solvation shell increases with increasing surface charge or ζ-potential. The low polydispersity index confirmed the absence of aggregation in solution at the relevant pH values.

Density of EDTA Groups. The amount of EDTA-silane groups on the surface of the nanoparticles was determined by CHN elemental analysis and TGA measurements (Table 1).

Table 1. Surface Group Fraction (FSG) for the Different Nanoparticles Measured by CHN Analysis and TGA

	CHN F_{SG}[a] (wt %)	TGA F_{SG} (wt %)	average (wt %)
Fe_3O_4(NOA)	6 ± 0.6	11	8.5 ± 0.6
Fe_3O_4(TMS-EDTA)	15 ± 2	17	16 ± 2
TiO_2(TMS-EDTA)	36 ± 3	42	39 ± 3
SiO_2(TMS-EDTA)	61 ± 5	50	55.5 ± 5

[a] F_{SG} = surface group fraction.

The weight loss during TGA measurements is a gradual process at first, due to interdigitation (entanglement) of the ligands, but around 400 °C a sudden drop in weight is observed, after which most of the TMS-EDTA is removed (Figure S8, Supporting Information). This observed weight loss can be directly translated into the surface group fraction (F_{SG}), which is the weight fraction of TMS-EDTA in the nanoparticle. Furthermore, the carbon and nitrogen weight fraction measured by CHN elemental analysis was also used to calculate the surface group fraction F_{SG}. Both methods (CHN and TGA) have their advantages, but each method induced a small error. The best approximation is to use the average of both measurements.

One of the aims of the research described in this paper was to investigate the influence of the sterical crowding of the immobilized ligand on the selectivity. Silane molecules can bind to the hydroxyl groups on the surface of the nanoparticles. This means that the density of TMS-EDTA groups on the nanoparticle is related to the initial density of hydroxyl groups on that oxide.[19,26,35] Three different oxides were selected with an increased affinity for silanes in the order Fe_3O_4 < TiO_2 < SiO_2.[36] The exact hydroxyl group density depends on several factors, including synthesis conditions, particle morphology and the nature of the crystalline phase.[26] This makes it difficult to give exact values, but approximate literature values can be used to get an idea of the relative abundance of hydroxyl groups on the surface of the different oxides.[19,26,29,35] The commercially available SiO_2 nanoparticles had the appearance of a very fine, flake-like powder. This type of silica is known to have a high hydroxyl group density on its surface especially in aqueous solution (6.0 − 8.0 μmol/m^2).[26] The commercially available TiO_2 nanoparticles consisted of type P25 TiO_2 (produced by Evonik Degussa) with a 80:20 anatase:rutile ratio and have an intermediate hydroxyl group density on their surface (4.6 μmol/m^2).[27] The Fe_3O_4 nanoparticles were covered with *n*-octylamine and are known to contain fewer OH groups on their surface (1.0−1.5 μmol/m^2).[28] The surface density (SD) of TMS-EDTA was approximated using eq 1:

$$\mathrm{SD}(\mu\mathrm{mol/m^2}) = \frac{\left(\frac{F_{SG}}{100}\right) r\rho}{3M_{SG}} \times 10^6 \quad (1)$$

where F_{SG} is the surface group fraction (wt %) (Table 1), M_{SG} is the molar mass of the surface group (345 g/mol), r is the particle radius (m) obtained by TEM measurements, and ρ the density (g/m^3) of the core material. For Fe_3O_4, SiO_2 and TiO_2, the densities are 5.1, 2.6 and 3.9 g/cm^3, respectively.[37] The diameters are 10.5 nm, 16.6 and 17.9 nm (TEM). From this data, the specific surface was calculated assuming spherical nanoparticles and the surface density of EDTA-silane groups indeed increases in the order Fe_3O_4 < TiO_2 < SiO_2 (Table 2).

Table 2. Calculated Specific Surface and Density of Functional Silanes on the Surface of the Different Nanoparticles Compared to the Initial Hydroxyl Group Density

	specific surface of the core (m^2/g)	OH[a] (μmol/m^2)	TMS-EDTA[b] (μmol/m^2)
Fe_3O_4	115	1.0−1.5	4.1
TiO_2	86	4.6	11.6
SiO_2	139	6.0−8.0	13.1

[a] Approximate hydroxyl group densities found in literature.[26−28] [b] Calculated surface density (SD) of TMS-EDTA, using eq 1.

The footprint of a silane molecule is about 0.32−0.38 nm^2.[38] This means that a perfect silane monolayer has an approximate surface density of 3 molecules/nm^2 (5 μmol/m^2). The higher surface density found for TiO_2(TMS-EDTA) and SiO_2(TMS-EDTA) (Table 2) means that there is a larger degree of oligomerization and multilayer formation. These are unavoidable phenomena when trialkylsilanes are used, even on surface of the less reactive Fe_3O_4 nanoparticles.[19,20,38]

Adsorption of Rare Earths. The adsorption of rare-earth ions from solution was investigated. The TMS-EDTA groups form the largest number of binding sites for metal ions, but metal ions can also bind nonspecifically to the deprotonated hydroxyl end groups on the hydrolyzed silanes or on the surface of the nanoparticle (Figure 5).[39] This is supported by the fact that the observed uptake of Gd^{3+} ions by TMS-EDTA functionalized nanoparticles is higher than the TMS-EDTA content on these nanoparticles (Table 3). The adsorption capacity is also pH dependent because both the EDTA carboxylic acid groups and hydroxyl groups are deprotonated at higher pH values.[39]

The influence of pH on the adsorption of Gd^{3+} was investigated (Figure 6). Gd^{3+} was chosen because it is located in the middle of the lanthanide series, which makes it a good model ion. An 8 mL solution containing 5 mg of nanoparticles and 3.75 × 10^{-3} M of Gd^{3+} was used (6 μmol/mg) to

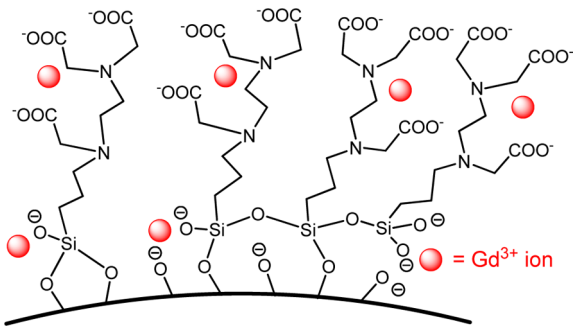

Figure 5. Schematic representation of the possible binding sites for metal ions (e.g., Gd^{3+}) on the surface of TMS-EDTA functionalized nanoparticles.

Table 3. Maximal Adsorption Capacity of the Fe_3O_4(TMS-EDTA), TiO_2(TMS-EDTA) and SiO_2(TMS-EDTA) Nanoparticles Compared with the Unfunctionalized Analogues and with Other Functionalized Nanoparticles in the Literature

particle(ligand)	core size (nm)	surface group (wt %)	ion	ion uptake (mg/g)
Fe_3O_4	10.5		Gd^{3+}	14
SiO_2	17.9		Gd^{3+}	20
TiO_2	16.6		Gd^{3+}	41
Fe_3O_4(TMS-EDTA)	10.5 ± 1.8	16 ± 2	Gd^{3+}	113 ± 6
TiO_2(TMS-EDTA)	17.9 ± 5.9	39 ± 3	Gd^{3+}	263 ± 11
SiO_2(TMS-EDTA)	16.6 ± 5.8	55.5 ± 5	Gd^{3+}	395 ± 32
Fe_3O_4(humic acid)[16]	14	15.5	Eu^{3+}	10.6
Fe_3O_4(DEHPA)[15]	N/A	13.9	La^{3+}	55.9
Fe_3O_4(EDTA)[7]	312.3	7.8	Cu^{2+}	46.3
Fe_3O_4(chitosan)[41]	13.5	4.9	Cu^{2+}	21.5
Fe_3O_4(dien)[42]	11.6	N/A	Cu^{2+}	12.43
GO(TMS-EDTA)[a][39]	N/A	N/A	Pb^{2+}	479

[a]Graphene oxide (GO) consists of graphene nanosheets with surface OH and COOH groups (high toxicity).[39]

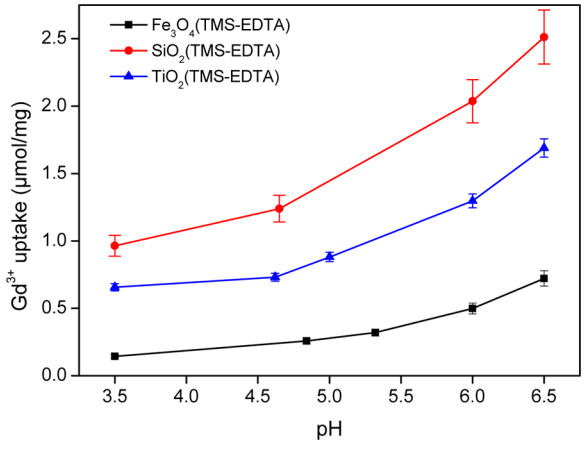

Figure 6. Uptake of Gd^{3+} ions by Fe_3O_4(TMS-EDTA), SiO_2(TMS-EDTA) and TiO_2(TMS-EDTA) nanoparticles as a function of pH.

guarantee an excess of rare-earth ions in order to obtain the maximal uptake capacity. The uptake of Gd^{3+} ions is the highest at pH 6.5 because of the increasingly deprotonated TMS-EDTA groups. Above pH 6.5, the solubility product of Gd^{3+} is exceeded ($K_{SP} = 10^{-24}$) and the Gd^{3+} ions in solution precipitate as $Gd(OH)_{3(s)}$ (Figure S10, Supporting Information).[40] The average uptake of rare-earth ions clearly increases in the order: SiO_2(TMS-EDTA) > TiO_2(TMS-EDTA) > Fe_3O_4(TMS-EDTA) due to the increasing amounts of EDTA-silane on the surface of these nanoparticle. The adsorption characteristics of several elements of the lanthanide series by Fe_3O_4(TMS-EDTA), SiO_2(TMS-EDTA) and TiO_2(TMS-EDTA) are shown in Figure 7. Single element solutions were

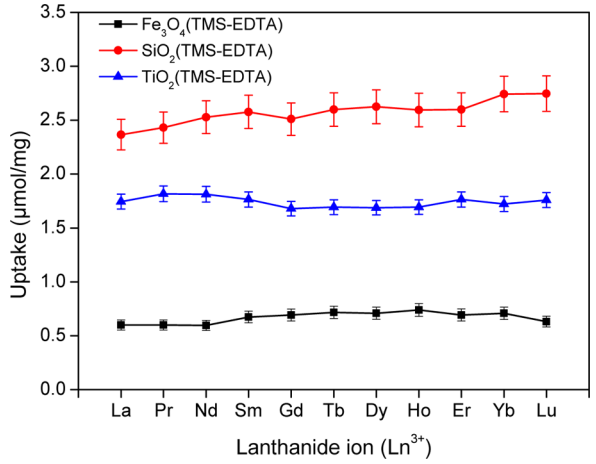

Figure 7. Uptake of rare-earth ions from single-element solutions by Fe_3O_4(TMS-EDTA), SiO_2(TMS-EDTA) and TiO_2(TMS-EDTA) nanoparticles at pH 6.3.

used with a large excess of rare-earth ion (6 μmol/mg) at pH 6.3 to obtain the highest possible uptake without precipitation. In the absence of competition between different ions, the uptake of the different lanthanide ions is quite similar (Figure 7). Furthermore, the stripping of rare-earth ions from Fe_3O_4(TMS-EDTA) nanoparticles was investigated. Complete stripping was observed after less than 5 min (Figure S13, Supporting Information) and a plateau value was reached at pH 3 with 98% stripping efficiency (Figure 8)). This is in good agreement with the fact that the carboxylic acid groups are fully protonated below pH 3 (ζ-potential > 0).

The stability of the different TMS-EDTA modified nanoparticles in acidic and alkaline solutions was tested. Nano-

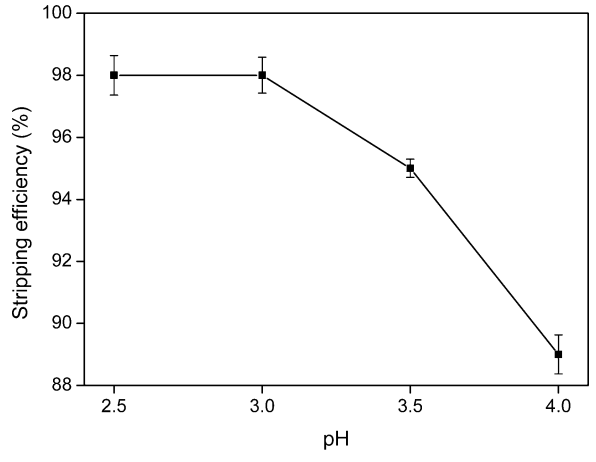

Figure 8. Stripping of Gd^{3+} from Fe_3O_4(TMS-EDTA) nanoparticles previously saturated with an excess of Gd^{3+} ions.

particles (10 mg) were dispersed in Milli-Q water (5 mL) and the pH was adjusted with a HCl (1 M) or NaOH (1 M) solution. The dispersion was then shaken for 24 h. The particles were removed from solution and the remaining metal content (Fe, Si or Ti) in the water was determined by TXRF analysis. Polypropylene sample carriers were used to determine the silicon content instead of the quartz sample carriers. The results show that the nanoparticles are stable between pH 2.5 and pH 10 (Figure 9). This wide pH window permits complex

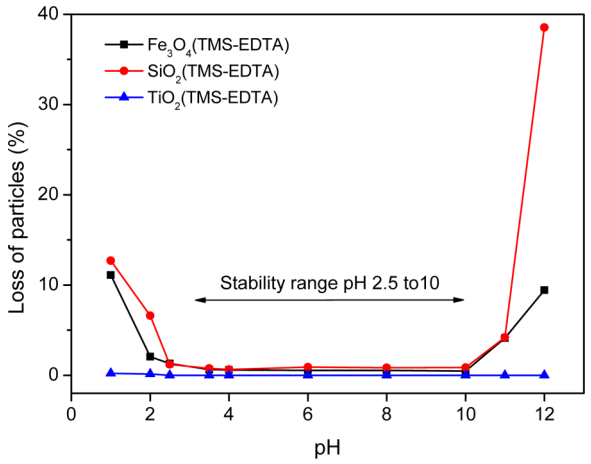

Figure 9. Nanoparticle stability in solutions with different pH values. The loss of particles after 24 h is shown as a function of pH.

formation and stripping of metal ions from the nanoparticles without damaging the nanoparticles, making this system reusable. Repeated adsorption (pH 6.5) and stripping (pH 2.75) cycles showed a negligible decrease in adsorption capacity after three cycles.

The adsorption capacity was compared with different functionalized nanoparticles reported in the literature (Table 3).[7,15,39,41−43] The functionalization of the nanoparticles with TMS-EDTA drastically increased the adsorption capacity. The lanthanide adsorption capacities (mg/g) are high compared to literature reports, this can be explained by the high surface group content and specific surface of these small nanoparticles and the low degree of aggregation, which keeps all the TMS-EDTA groups available.[7,15] Lighter materials (TiO_2 and SiO_2) with a higher EDTA density have even larger adsorption capacities (mg/g). This is why Madadrang et al. showed record adsorption capacities of 479 mg/g for Pb^{2+} on the very light graphene-oxide sheets functionalized with TMS-EDTA.[39] Few nanoparticle sorbents have been used for the adsorption of lanthanide ions, so the results were compared with the ion showing a maximal adsorption capacity for each system.

Separation of Rare Earths. The selectivity was reported using the enrichment factor (EF), which compares the molar ratio of two elements A and B before and after separation, according to eq 2. B was always chosen to be the heavier of the two rare earths because this results in an enrichment factor >1, which is easier to work with. The ratio B/A after separation was determined directly on the nanoparticles using TXRF. Because the metal ions can be full striped from the nanoparticles, the ratio on the nanoparticles is the same ratio that can be found when measuring the stripping solution.

$$\mathrm{EF} = \frac{(B/A)_{\text{after separation}}}{(B/A)_{\text{before separation}}} = \frac{(B/A)_{\text{on the nanoparticles}}}{(B/A)_{\text{feed solution}}} \quad (2)$$

The working conditions were optimized for the separation experiments. Tests showed that the rare-earth ions had to be added in excess compared to the amount of EDTA groups on the nanoparticles in solution (Figure S11, Supporting Information). Without an excess of rare-earth ions in solution, the EDTA groups captured every ion in solution without much selectivity. The influence of the counterion (nitrate or chloride salts) was negligible (Figure S12, Supporting Information). The influence of pH is illustrated in Figure 10. The separation of

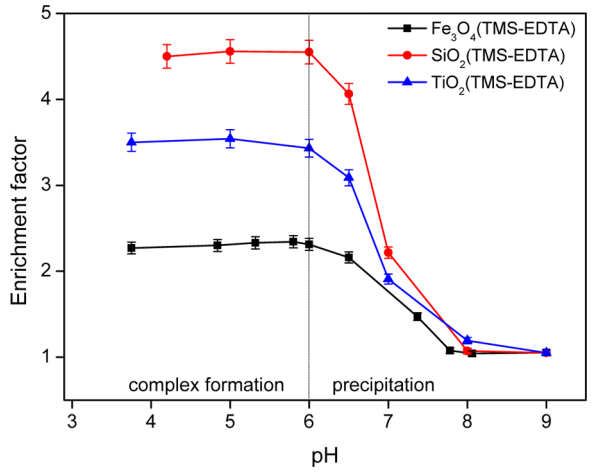

Figure 10. Separation of La^{3+} and Er^{3+} by different EDTA-functionalized nanoparticles at different pH values.

La^{3+}/Er^{3+} was chosen because the large difference in selectivity helps visualizing a possible trend. The solution contained 3 μmol of each rare earth per mg of nanoparticles (a large excess, see Figure 7). The selectivity of the system does not change much in the range between pH 4 and 6. A high pH is desirable to increase the adsorption of rare-earth ions (Figure 6), so the separation of rare-earth ions is therefore best carried out between pH 6 and 6.5, to ensure a maximal uptake of rare-earth ions with high selectivity. Beyond pH 6.5, precipitation of rare-earth hydroxides occurred.

Influence of Sterical Crowding on the Selectivity. It is well-known that EDTA and other metal chelating compounds have an inherent selectivity.[24,44,45] However, because the EDTA groups on the nanoparticles are, in principle identical, one would not expect additional differences in selectivity, depending on which substrate the TMS-EDTA is attached to. The difference in selectivity between the different nanoparticles is therefore definitely the most remarkable observation to be made (Figure 10). It is assumed that this effect originates from the fact that Fe_3O_4, TiO_2 and SiO_2 nanoparticles have increasingly high densities of TMS-EDTA on their surface (Table 2). The denser the EDTA coating, the more the selectivity increases toward the smaller Er^{3+} ion and decreases toward the larger La^{3+} ion. This could originate from the fact that a dense EDTA-silane (multi)layer is more impenetrable for larger ions or from the fact that the size of the EDTA cage is reduced due to sterical crowding caused by the high density of EDTA groups on the surface of the nanoparticle. Thermodynamic models exist to describe the complex interactions between neighboring metal ions in polynuclear complexes.[46−52]

dx.doi.org/10.1021/am406027y | ACS Appl. Mater. Interfaces 2014, 6, 4980−4988

However, determining the exact structure and speciation of the dense EDTA-silane layer on the surface of the nanoparticles is not as straightforward as for chelating complexes in solution. Quantifying the interactions between rare-earth ions within the dense EDTA-silane layer is therefore too complex to attempt here. Instead, experimental evidence is proposed to support this theory of a size-based selectivity related to the density of ligands on the surface of the nanoparticles.

This effect was further investigated by looking at the separation of La^{3+} ions from other trivalent lanthanide ions (Ln^{3+}) (Figure 11). As expected, the enrichment factors

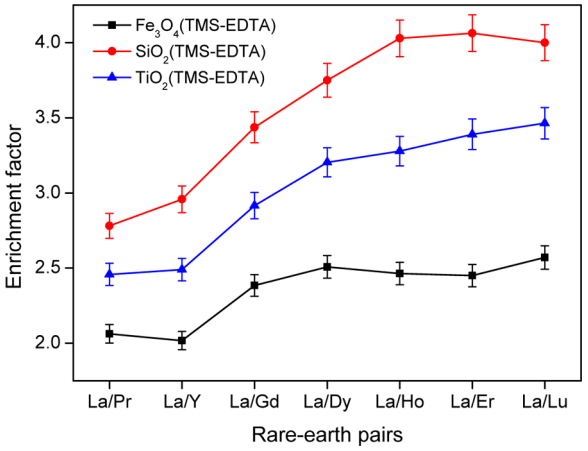

Figure 11. Separation of La^{3+}/Ln^{3+} rare-earth pairs (pH 6.5) with increasingly different ionic radii from left to right.

increased with increasing difference in ionic radius, but it is also evident that TiO_2(TMS-EDTA) and SiO_2(TMS-EDTA) have a higher selectivity toward smaller (heavier) ions than Fe_3O_4(TMS-EDTA). In addition, SiO_2(TMS-EDTA) shows the steepest increase in enrichment factor over the series, which can be explained by the fact that it has the largest density of TMS-EDTA on its surface. TiO_2(TMS-EDTA) and Fe_3O_4(TMS-EDTA) show a less steep increase in enrichment factor because their EDTA-coating is less dense and therefore less capable of size-based selectivity due to sterical crowding.

Large differences in enrichment factors (EF) for different nanoparticles were only found for rare-earth pairs containing lanthanum (Figure 11), possibly because La^{3+} is the only ion that is large enough to trigger the selectivity due to the density of EDTA groups on the surface. Note that EDTA has an inherent selectivity toward the heavier (smaller) lanthanide ions, so that any selectivity arising from the difference in surface density is only observable if it is large enough compared to the inherent selectivity of EDTA. For the other rare-earth ions, the difference was much smaller. The Lu^{3+}/Ln^{3+} series (Figure S15, Supporting Information) and Pr^{3+}/Ln^{3+} series (Figure S16, Supporting Information), for example, both showed some difference in selectivity, but the effect was not as large as that for La^{3+}/Ln^{3+} (Figure 11). The position of yttrium in the separation series was elucidated by looking at the yttrium separation series (Figure S14, Supporting Information). It is evident that Y^{3+} behaves like Pr^{3+} or Nd^{3+} in our system (EF = 1), even though the ionic radius of Y^{3+} is closer to that of Ho^{3+}.[53] This is in agreement with previous reports on the complex formation of lanthanide ions with EDTA and HEDTA in solution.[24] The "itinerant" behavior of Y^{3+} is a phenomenon that describes the fact that Y^{3+} can move across the lanthanide series, depending on the extraction system.[44]

4. CONCLUSION

Magnetic (Fe_3O_4) and nonmagnetic (TiO_2 and SiO_2) nanoparticles were coated with EDTA-silane and their adsorption capacity and selectivity toward rare-earth ions was investigated. The covalently bonded TMS-EDTA protects the surface of the nanoparticles from oxidation and provides surface charges to prevent aggregation. The high adsorption capacities (100 to 400 mg/g) of these nanoparticles is due to their small diameter (10 to 20 nm) and high surface area (85 to 140 m^2/g), combined with a large coverage of TMS-EDTA. It was found that the selectivity toward smaller rare-earth ions increased in the same order as the density of the EDTA-silane on the surface, namely Fe_3O_4(TMS-EDTA) < TiO_2(TMS-EDTA) < SiO_2(TMS-EDTA). This observation could be used to tune the selectivity of other existing extractants and further research will be directed to explore this phenomenon of selectivity enhancement by steric crowding. The main advantage of magnetic nanoparticles is the fact that they can be easily retrieved from solution using a small magnet. On the other hand, SiO_2 and TiO_2 nanoparticles can hold larger quantities of TMS-EDTA on their surface and can therefore adsorb more rare-earth ions, but their removal from solution is more tedious. This knowledge about the differences in adsorption capacity and selectivity of TMS-EDTA attached to these different oxides could prove valuable for the future design of Fe_3O_4@SiO_2 or Fe_3O_4@TiO_2 core–shell nanoparticles. These hybrid materials with a magnetic Fe_3O_4 core and a nonmagnetic shell could combine the convenience of magnetic retrieval with the high adsorption capacity and selectivity of SiO_2-based nanoparticles.

■ ASSOCIATED CONTENT

Supporting Information

DLS, VSM, TGA measurements, FTIR spectra, and TEM pictures. Graphs showing the precipitation threshold for adsorption experiments, the effect of counterion on separation efficiency, the influence of the rare-earth/EDTA ratio on the selectivity, the influence of stripping time, and some additional graphs showing the separation of various rare-earths pairs. This material is available free of charge via the Internet at http://pubs.acs.org.

■ AUTHOR INFORMATION

Corresponding Author

*K. Binnemans. E-mail: Koen.Binnemans@chem.kuleuven.be.

Notes

The authors declare no competing financial interest.

■ ACKNOWLEDGMENTS

The authors thank the KU Leuven (projects GOA/13/008 and IOF-KP RARE^3) and the FWO Flanders (Ph.D. fellowship to D.D. and research project G.0618.11 N) for financial support. CHN analyses were performed by Dirk Henot, DLS and ζ-potential measurements by Dr. Naveen K. Reddy and TGA measurements by Danny Winant and Dr. Stijn Schaltin.

■ REFERENCES

(1) Hao, R.; Xing, R.; Xu, Z.; Hou, Y.; Gao, S.; Sun, S. Synthesis, Functionalization, and Biomedical Applications of Multifunctional Magnetic Nanoparticles. *Adv. Mater.* **2010**, *22*, 2729–2742.

(2) Lu, A.-H.; Salabas, E. L.; Schüth, F. Magnetic Nanoparticles: Synthesis, Protection, Functionalization, and Application. *Angew. Chem., Int. Ed.* **2007**, *46*, 1222−1244.
(3) Liu, Z.; Li, B.; Wang, B.; Yang, Z.; Wang, Q.; Li, T.; Qin, D.; Li, Y.; Wang, M.; Yan, M. Magnetic Nanoparticles Modified with DTPA-AMC-Rare Earth for Fluorescent and Magnetic Resonance Dual Mode Imaging. *Dalton Trans.* **2012**, *41*, 8723−8728.
(4) Wang, B.; Hai, J.; Wang, Q.; Li, T.; Yang, Z. Coupling of Luminescent Terbium Complexes to Fe_3O_4 Nanoparticles for Imaging Applications. *Angew. Chem., Int. Ed.* **2011**, *50*, 3063−3066.
(5) Xi, P.; Cheng, K.; Sun, X.; Zeng, Z.; Sun, S. Magnetic Fe_3O_4 Nanoparticles Coupled with a Fluorescent Eu Complex for Dual Imaging Applications. *Chem. Commun.* **2012**, *48*, 2952−2954.
(6) Goon, I. Y.; Zhang, C.; Lim, M.; Gooding, J. J.; Amal, R. Controlled Fabrication of Polyethylenimine-Functionalized Magnetic Nanoparticles for the Sequestration and Quantification of Free Cu^{2+}. *Langmuir* **2010**, *26*, 12247−12252.
(7) Liu, Y.; Chen, M.; Yongmei, H. Study on the Adsorption of Cu(II) by EDTA Functionalized Fe_3O_4 Magnetic Nano-Particles. *Chem. Eng. J.* **2013**, *218*, 46−54.
(8) Ren, Y.; Abbood, H. A.; He, F.; Peng, H.; Huang, K. Magnetic EDTA-modified Chitosan/SiO_2/Fe_3O_4 Adsorbent: Preparation, Characterization, and Application in Heavy Metal Adsorption. *Chem. Eng. J.* **2013**, *226*, 300−311.
(9) Sun, L.; Li, Y.; Sun, M.; Wang, H.; Xu, S.; Zhang, C.; Yang, Q. Porphyrin-Functionalized Fe_3O_4@SiO_2 Core/Shell Magnetic Colorimetric Material for Detection, Adsorption and Removal of Hg^{2+} in Aqueous Solution. *New J. Chem.* **2011**, *35*, 2697−2704.
(10) Warner, C. L.; Addleman, R. S.; Cinson, A. D.; Droubay, T. C.; Engelhard, M. H.; Nash, M. A.; Yantasee, W.; Warner, M. G. High-Performance, Superparamagnetic, Nanoparticle-Based Heavy Metal Sorbents for Removal of Contaminants from Natural Waters. *ChemSusChem* **2010**, *3*, 749−757.
(11) Rossier, M.; Koehler, F. M.; Athanassiou, E. K.; Grass, R. N.; Aeschlimann, B.; Gunther, D.; Stark, W. J. Gold Adsorption on the Carbon Surface of C/Co Nanoparticles Allows Magnetic Extraction from Extremely Diluted Aqueous Solutions. *J. Mater. Chem.* **2009**, *19*, 8239−8243.
(12) Rossier, M.; Koehler, F. M.; Athanassiou, E. K.; Grass, R. N.; Waelle, M.; Birbaum, K.; Günther, D.; Stark, W. J. Energy-Efficient Noble Metal Recovery by the Use of Acid-stable Nanomagnets. *Ind. Eng. Chem. Res.* **2010**, *49*, 9355−9362.
(13) Yantasee, W.; Warner, C. L.; Sangvanich, T.; Addleman, R. S.; Carter, T. G.; Wiacek, R. J.; Fryxell, G. E.; Timchalk, C.; Warner, M. G. Removal of Heavy Metals from Aqueous Systems with Thiol Functionalized Superparamagnetic Nanoparticles. *Environ. Sci. Technol.* **2007**, *41*, 5114−5119.
(14) Hao, Y.-M.; Man, C.; Hu, Z.-B. Effective Removal of Cu (II) Ions from Aqueous Solution by Amino-functionalized Magnetic Nanoparticles. *J. Hazard. Mater.* **2010**, *184*, 392−399.
(15) Wu, D.; Sun, Y.; Wang, Q. Adsorption of Lanthanum (III) from Aqueous Solution Using 2-ethylhexyl Phosphonic Acid Mono-2-ethylhexyl Ester-Grafted Magnetic Silica Nanocomposites. *J. Hazard. Mater.* **2013**, *260*, 409−419.
(16) Yang, S.; Zong, P.; Ren, X.; Wang, Q.; Wang, X. Rapid and Highly Efficient Preconcentration of Eu(III) by Core−Shell Structured Fe_3O_4@Humic Acid Magnetic Nanoparticles. *ACS Appl. Mater. Interfaces* **2012**, *4*, 6891−6900.
(17) Li, Y.; Wu, J.; Qi, D.; Xu, X.; Deng, C.; Yang, P.; Zhang, X. Novel Approach for the Synthesis of Fe_3O_4@TiO_2 Core-Shell Microspheres and their Application to the Highly Specific Capture of Phosphopeptides for MALDI-TOF MS Analysis. *Chem. Commun.* **2008**, 564−566.
(18) Tucker-Schwartz, A. K.; Farrell, R. A.; Garrell, R. L. Thiol−ene Click Reaction as a General Route to Functional Trialkoxysilanes for Surface Coating Applications. *J. Am. Chem. Soc.* **2011**, *133*, 11026−11029.
(19) De Palma, R.; Peeters, S.; Van Bael, M. J.; Van den Rul, H.; Bonroy, K.; Laureyn, W.; Mullens, J.; Borghs, G.; Maes, G. Silane Ligand Exchange to Make Hydrophobic Superparamagnetic Nanoparticles Water-Dispersible. *Chem. Mater.* **2007**, *19*, 1821−1831.
(20) Larsen, B. A.; Hurst, K. M.; Ashurst, W. R.; Serkova, N. J.; Stoldt, C. R. Mono and Dialkoxysilane Surface Modification of Superparamagnetic Iron Oxide Nanoparticles for Application as Magnetic Resonance Imaging Contrast Agents. *J. Mater. Res.* **2012**, *27*, 1846−1852.
(21) Bloemen, M.; Brullot, W.; Luong, T. T.; Geukens, N.; Gils, A.; Verbiest, T. Improved Functionalization of Oleic Acid-Coated Iron Oxide Nanoparticles for Biomedical Applications. *J. Nanopart. Res.* **2012**, *14*, 1100−1010.
(22) Hermanson, G. T. In *Bioconjugate Techniques*, 2nd ed.; Hermanson, G. T., Ed.; Academic Press: New York, 2008; pp 562−581.
(23) Xie, F.; Zhang, T. A.; Dreisinger, D.; Doyle, F. A critical review on solvent extraction of rare earths from aqueous solutions. *Miner. Eng.* **2014**, *56*, 10−28.
(24) Choppin, G. R.; Goedken, M. P.; Gritmon, T. F. The Complexation of Lanthanides by Aminocarboxylate Ligands - II. *J. Inorg. Nucl. Chem.* **1977**, *39*, 2025−2030.
(25) Vander Hoogerstraete, T.; Onghena, B.; Binnemans, K. Homogeneous Liquid−Liquid Extraction of Rare Earths with the Betaine−Betainium Bis(trifluoromethylsulfonyl)imide Ionic Liquid System. *Int. J. Mol. Sci.* **2013**, *14*, 21353−21377.
(26) Dugas, V.; Chevalier, Y. Surface Hydroxylation and Silane Grafting on Fumed and Thermal Silica. *J. Colloid Interface Sci.* **2003**, *264*, 354−361.
(27) Mueller, R.; Kammler, H. K.; Wegner, K.; Pratsinis, S. E. OH Surface Density of SiO_2 and TiO_2 by Thermogravimetric Analysis. *Langmuir* **2002**, *19*, 160−165.
(28) Cornell, R. M.; Schwertmann, U. *The Iron Oxides: Structure, Properties, Reactions, Occurrences and Uses*, 2nd ed.; Wiley-VCH: Weinheim, 2003; Chapter 10, pp 221−235.
(29) Zhao, J.; Milanova, M.; Warmoeskerken, M. M. C. G.; Dutschk, V. Surface Modification of TiO_2 Nanoparticles with Silane Coupling Agents. *Colloids Surf., A* **2012**, *413*, 273−279.
(30) Brullot, W.; Reddy, N. K.; Wouters, J.; Valev, V. K.; Goderis, B.; Vermant, J.; Verbiest, T. Versatile Ferrofluids Based on Polyethylene Glycol Coated Iron Oxide Nanoparticles. *J. Magn. Magn. Mater.* **2012**, *324*, 1919−1925.
(31) Anderson, D. R. In *Analysis of Silicones*; Smith, A. L., Ed.; Wiley-Interscience: New York, 1974; p 10.
(32) Kosmulski, M. pH-Dependent Surface Charging and Points of Zero Charge. II. Update. *J. Colloid Interface Sci.* **2004**, *275*, 214−224.
(33) Kosmulski, M. pH-Dependent Surface Charging and Points of Zero Charge. III. Update. *J. Colloid Interface Sci.* **2006**, *298*, 730−741.
(34) Kosmulski, M. *Surface Charging and Point of Zero Charge*; CRC Press: Boca Raton, FL, 2009.
(35) Huang, X.; Schmucker, A.; Dyke, J.; Hall, S. M.; Retrum, J.; Stein, B.; Remmes, N.; Baxter, D. V.; Dragnea, B.; Bronstein, L. M. Magnetic Nanoparticles with Functional Silanes: Evolution of Well-Defined Shells from Anhydride Containing Silane. *J. Mater. Chem.* **2009**, *19*, 4231−4239.
(36) Witucki, G. L. A Silane Primer - Chemistry and Applications of Alkoxy Silanes. *J. Coat. Technol.* **1993**, *65*, 57−60.
(37) Harrison, R. D.; Ellis, H. *Book of Data*; Longman: Edinburgh Gate, U.K., 1984; p 166.
(38) Fadeev, A. Y.; McCarthy, T. J. Self-Assembly Is Not the Only Reaction Possible Between Alkyltrichlorosilanes and Surfaces: Monomolecular and Oligomeric Covalently Attached Layers of Dichloro- and Trichloroalkylsilanes on Silicon. *Langmuir* **2000**, *16*, 7268−7274.
(39) Madadrang, C. J.; Kim, H. Y.; Gao, G.; Wang, N.; Zhu, J.; Feng, H.; Gorring, M.; Kasner, M. L.; Hou, S. Adsorption Behavior of EDTA-Graphene Oxide for Pb (II) Removal. *ACS Appl. Mater. Interfaces* **2012**, *4*, 1186−1193.
(40) Diakonov, I. I.; Ragnarsdottir, K. V.; Tagirov, B. R. Standard Thermodynamic Properties and Heat Capacity Equations of Rare Earth Hydroxides:: II. Ce(III)-, Pr-, Sm-, Eu(III)-, Gd-, Tb-, Dy-, Ho-,

Er-, Tm-, Yb-, and Y-Hydroxides. Comparison of Thermochemical and Solubility Data. *Chem. Geol.* **1998**, *151*, 327−347.
(41) Chang, Y.-C.; Chen, D.-H. Preparation and Adsorption Properties of Monodisperse Chitosan-Bound Fe_3O_4 Magnetic Nanoparticles for Removal of Cu(II) Ions. *J. Colloid Interface Sci.* **2005**, *283*, 446−451.
(42) Huang, S.-H.; Chen, D.-H. Rapid Removal of Heavy Metal Cations and Anions from Aqueous Solutions by an Amino-functionalized Magnetic Nano-Adsorbent. *J. Hazard. Mater.* **2009**, *163*, 174−179.
(43) Liu, J.-f.; Zhao, Z.-s.; Jiang, G.-b. Coating Fe_3O_4 Magnetic Nanoparticles with Humic Acid for High Efficient Removal of Heavy Metals in Water. *Environ. Sci. Technol.* **2008**, *42*, 6949−6954.
(44) Collier, D. C. The Itinerant Position of Yttrium as Evidenced by Carboxylic Acid Extraction. Ph.D. thesis, University of Tennessee, Knoxville, TN, 2012.
(45) Huang, C.-H. *Rare Earth Coordination Chemistry: Fundamentals and Applications*; Wiley: Singapore, 2010.
(46) Arago, J.; Bencini, A.; Bianchi, A.; Garcia-Espana, E.; Micheloni, M.; Paoletti, P.; Ramirez, J. A.; Paoli, P. Interaction of "Long" Open-Chain Polyazaalkanes with Hydrogen and Copper(II) Ions. *Inorg. Chem.* **1991**, *30*, 1843−1849.
(47) Koper, G. J. M.; van Duijvenbode, R. C.; Stam, D. D. P. W.; Steuerle, U.; Borkovec, M. Synthesis and Protonation Behavior of Comblike Poly(ethyleneimine). *Macromolecules* **2003**, *36*, 2500−2507.
(48) Borkovec, M.; Hamacek, J.; Piguet, C. Statistical Mechanical Approach to Competitive Binding of Metal Ions to Multi-Center Receptors. *Dalton Trans.* **2004**, 4096−4105.
(49) Dalla-Favera, N.; Hamacek, J.; Borkovec, M.; Jeannerat, D.; Ercolani, G.; Piguet, C. Tuneable Intramolecular Intermetallic Interactions as a New Tool for Programming Linear Heterometallic 4f−4f Complexes. *Inorg. Chem.* **2007**, *46*, 9312−9322.
(50) Riis-Johannessen, T.; Dalla Favera, N.; Todorova, T. K.; Huber, S. M.; Gagliardi, L.; Piguet, C. Understanding, Controlling and Programming Cooperativity in Self-Assembled Polynuclear Complexes in Solution. *Chem.—Eur. J.* **2009**, *15*, 12702−12718.
(51) Dalla Favera, N.; Kiehne, U.; Bunzen, J.; Hytteballe, S.; Lützen, A.; Piguet, C. Intermetallic Interactions Within Solvated Polynuclear Complexes: A Misunderstood Concept. *Angew. Chem., Int. Ed.* **2010**, *49*, 125−128.
(52) Zaim, A.; Favera, N. D.; Guenee, L.; Nozary, H.; Hoang, T. N. Y.; Eliseeva, S. V.; Petoud, S.; Piguet, C. Lanthanide Hexafluoroacetylacetonates vs. Nitrates for the Controlled Loading of Luminescent Polynuclear Single-Stranded Oligomers. *Chem. Sci.* **2013**, *4*, 1125−1136.
(53) Cotton, S. In *Lanthanide and Actinide Chemistry*; Woolins, D., Crabtree, B., Atwood, D., Meyer, G., Eds.; Wiley: Chichester, U.K., 2006; Chapter 4, pp 35−60.